JOURNAL OF SOLID STATE CHEMISTRY **129,** 214–222 (1997)
ARTICLE NO. SC967215

A New Collapsed Structure Related to the 2212 Structure: HREM Study of $Bi_{12}Sr_{18}Fe_{10}O_{52}$

M. Hervieu, O. Pérez, D. Groult, D. Grebille, H. Leligny, and B. Raveau

Laboratoire CRISMAT, ISMRA/Université de Caen, 6 Boulevard du Maréchal Juin, 14050 Caen Cedex, France

Received July 19, 1996; in revised form October 30, 1996; accepted November 6, 1996

A shearing mechanism strategy is applied to a 2212-type ferrite. A new compound is obtained, which exhibits a monoclinic cell with the refined parameters $a = 16.491(9)$ Å, $b = 5.481(3)$ Å, $c = 30.086(16)$ Å, and $\beta = 91°39(2)$ and the space group $P2_1/n$. This structure can be described as the member m = 4 of the general family $^{[011]}[Bi_2Sr_3Fe_2O_9]_m[Bi_{4-x}Sr_6Fe_{2+x}O_{16-\delta}]$. It consists of "2212"-type slices, parallel to $(011)_{2212}$, four FeO_6 octahedra thick, interconnected through $[Bi_{4-x}Sr_6Fe_{2+x}O_{16}]$ slices that are two FeO_6 octahedra thick and that involve BiO_5 bipyramids. The HREM study of the crystals allowed to understand the structural mechanisms which generate this structure and govern the nonstoichiometry. Fe for Bi substitution, intergrowth defects, mixed crystallographic shear planes, and 3212 defective members are characterized. The relationships with the homologous copper-based collapsed phase and the other layered structures of the system are discussed. © 1997 Academic Press

INTRODUCTION

The Bi–Sr–Cu–O and Bi–Sr–Fe–O systems exhibit great similarities, especially in their ability to form layered oxides, where a double $[(BiO)_2]$ layer is systematically sandwiched between two [SrO] layers. $Bi_2Sr_3Fe_2O_9$ (1) is closely related to the so-called 2212 $Bi_2Sr_2CaCu_2O_8$ (2, 3), since both structures are built up from the intergrowth of one triple rock salt-type layer, $[(BiO)_2(SrO)]$, and one double perovskite-type layer, $[Sr_2Fe_2O_6]$ or $[SrCaCu_2O_5]$. Moreover, it was shown that they both exhibit an incommensurate modulated structure (1, 4–8). The two structures only differ in the nature of the iron and copper layers, which are double octahedral layers for $Bi_2Sr_3Fe_2O_9$, whereas they are pyramidal for $Bi_2Sr_2CaCu_2O_8$. In the same way, $Bi_2Sr_4Fe_3O_{11}$ (9) can be compared to the 2223 structure (10) $Bi_{2-x}Pb_xSr_2Ca_2Cu_3O_{10}$. It appears also that the possibilities for building up complex intergrowths between layered structures are wider with the ferrites than with the cuprates. $Bi_2Sr_4Fe_2O_{10}$ can be described from the intergrowth of one 2201-type layer with one 0201-type layer. It is the first member of a new structural family $Bi_{n+1}Sr_{2n+2}Ba_{n-1}Fe_{n+1}O_{6n+4}$ (11). In contrast, the copper based homologues are hardly stabilized in the form of single phases and are mainly observed as extended defects. This is partly due to the necessity of introducing calcium or rare earth cations to stabilize the 2212 copper oxide and to the stability of the monoclinic collapsed phase $Bi_{17}Sr_{16}Cu_7O_{49}$ (14), directly related to the 2201's, which is easily formed as soon as the synthesis conditions are not exactly those needed for the 2201.

At the same time, the shearing mechanism strategy, which was studied a long time ago for the generation of oxides derived from rutile and tungsten trioxide structures (see Ref. (13) for review), was proved to be an efficient way to generate new bismuth copper-based oxides or oxycarbonates (10, 14–18). Starting from the parent structures $Bi_2Sr_2CuO_{6+\delta}$ (2201), $Bi_2Sr_2CaCu_2O_{8+\delta}$ (2212), or $Bi_2Sr_4Cu_2CO_3O_8$, new shear-like structures can be generated by theoretically applying a shearing mechanism. $Bi_{16}Sr_{28}Cu_{17}O_{69}$ (14) can thus be described as a 2212-double collapsed structure, the crystallographic shear plane being $\{011\}_{2212}$. Such a structural mechanism was also observed in the bismuth iron-based oxides so that the ferrite $Bi_{13}Ba_2Sr_{25}Fe_{13}O_{66}$ (18) can be described as a double collapsed structure derived from the "2201/0201".

One of the interesting structural characteristics of these collapsed bismuth phases is that the infinite double $[(BiO)_2]$ layers do not exist any more. In fact, the shearing mechanism along $\mathbf{c}_{2201}$ and $\mathbf{c}_{2212}$ causes these layers to be interrupted and connected to layers of different natures. In that way, "stairlike" (Bi_2O_2) layers are formed and the width of the "stair," i.e., the length of the Bi segments, is strongly dependent of the nominal composition of each of these phases.

This paper deals with the electron microscopy study of a few ferrite, $Bi_{12}Sr_{18}Fe_{10}O_{52}$, which will be described as a double collapsed 2212 ferrite. This study was carried out in parallel with an X-ray diffraction study on a single crystal, which will be detailed elsewhere (19).

0022-4596/97 $25.00

EXPERIMENTAL

The powder samples were prepared from a mixture of the starting materials Bi_2O_3, Fe_2O_3, and $Sr(NO_3)_2$ weighed in the molar ratio 0.95 : 1 : 3. The mixture was heated in an alumina crucible in air for 48 hr, at 850°C and then analyzed by X-ray powder diffraction (XRD). Single crystals were grown from a charge containing the same starting materials but weighed in the molar ratio 0.66 : 0.50 : 2. About 10 g of the charge was first heated at 850°C for 2 hr, held at this temperature for 24 hr, then heated up to 1050°C over 1 hr, held for 2 hr, and slowly cooled down to 950°C at a rate of 1°C/hr. The charge was finally cooled to 20°C in 5 hr. This procedure produced small black needles typically 0.2–1 mm long and a few tens of micrometers thick.

The single crystals were identified by means of Weissenberg photographs and used for X-ray diffraction and electron microscopy studies.

X-ray diffraction data were collected at ESRF (Grenoble) using the synchrotron source on the beam line 2ID11.

The electron microscopy study was carried out on the powder sample and on two selected single crystals, crushed in alcohol. The microcrystals in suspension were deposited on a holey carbon film. The electron diffraction (ED) study was performed with a JEOL 200CX electron microscope fitted with a eucentric goniometer ($\pm$ 60°). The high resolution electron microscopy (HREM) study was performed with a TOPCON 002B microscope having a point resolution of 1.8 Å. Both microscopes are equipped with EDS analysers. The theoretical images were calculated using the MacTempas program.

RESULTS

According to the above mentioned experimental process, the powder X-ray patterns show that a single phased sample is obtained. The reconstruction of the reciprocal space, by ED, evidences monoclinic symmetry. Choosing a cell with $\beta \approx 90°$, the parameters were refined from XRD data (19) to

$$a = 16.491\,(9)\ \text{Å} \quad b = 5.481\,(3)\ \text{Å} \quad c = 30.086\,(16)\ \text{Å}$$

$$\text{and} \quad \beta = 91°39\,(2).$$

The conditions limiting the reflection are $h0l$, $h + l = 2n$ and $0k0$, $k = 2n$, compatible with the space group $P2_1/n$. A [010] ED pattern is given in Fig. 1. In fact, for crystallites of the powder samples, streaks are sometimes observed along c^*, which are generated by intergrowth defects. Their existence results from composition inhomogeneities. In the crushed single crystals, the reflections are sharp and well defined. This pattern is close to those registered for the double collapsed 2201/0201 phases, $Bi_{13}Ba_2Sr_{25}Fe_{13}O_{66}$ (18) and $Bi_{16}Sr_{28}Cu_{17}O_{69}$ (14), suggesting that a shearing mechanism also takes place in the matrix.

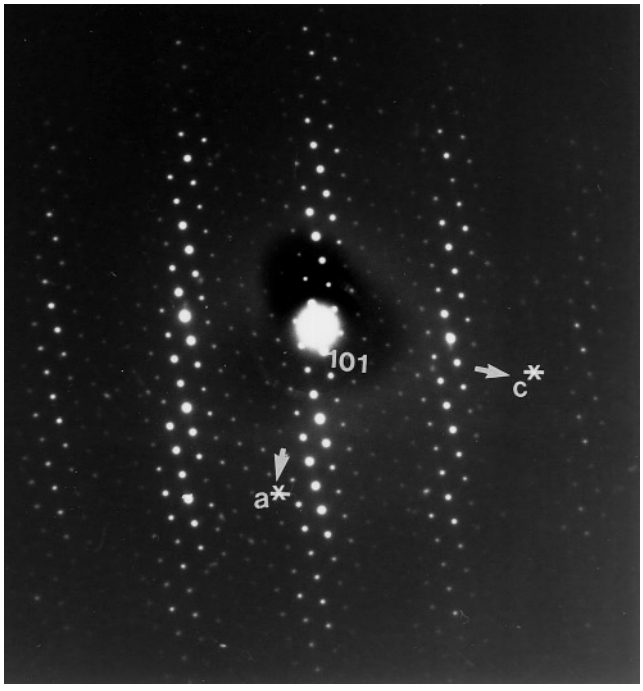

FIG. 1. [010] ED pattern of the ferrite 2212 collapsed structure.

The EDS analyses were performed on numerous microcrystals. When the ED patterns attest that there are no (or few) extended defects in the matrix, the actual average composition of the grains was observed to be $Bi_{2.2}Sr_{3.5}Fe_{2.3}$. This is also the composition corresponding to the crushed single crystals.

Regular Structure

In such complex layered structures, the structural mechanism can be understood easily from the [010] HREM images. The images registered on the thin crystal edges, for a focus value close to -550 Å where the cation positions are highlighted, allow a direct interpretation to be made. An example of enlarged image is given in Fig. 2a. Such [010] images clearly show the stair-like configuration of double bismuth layers, typical of the sheared and collapsed structures. The characteristics of the new structure are the following:

(i) The structure is built up from the stacking of slices parallel to (001). Three of them are indicated in the bottom part of the micrograph. The monoclinic cell is outlined in the structure projection of Fig. 2b.

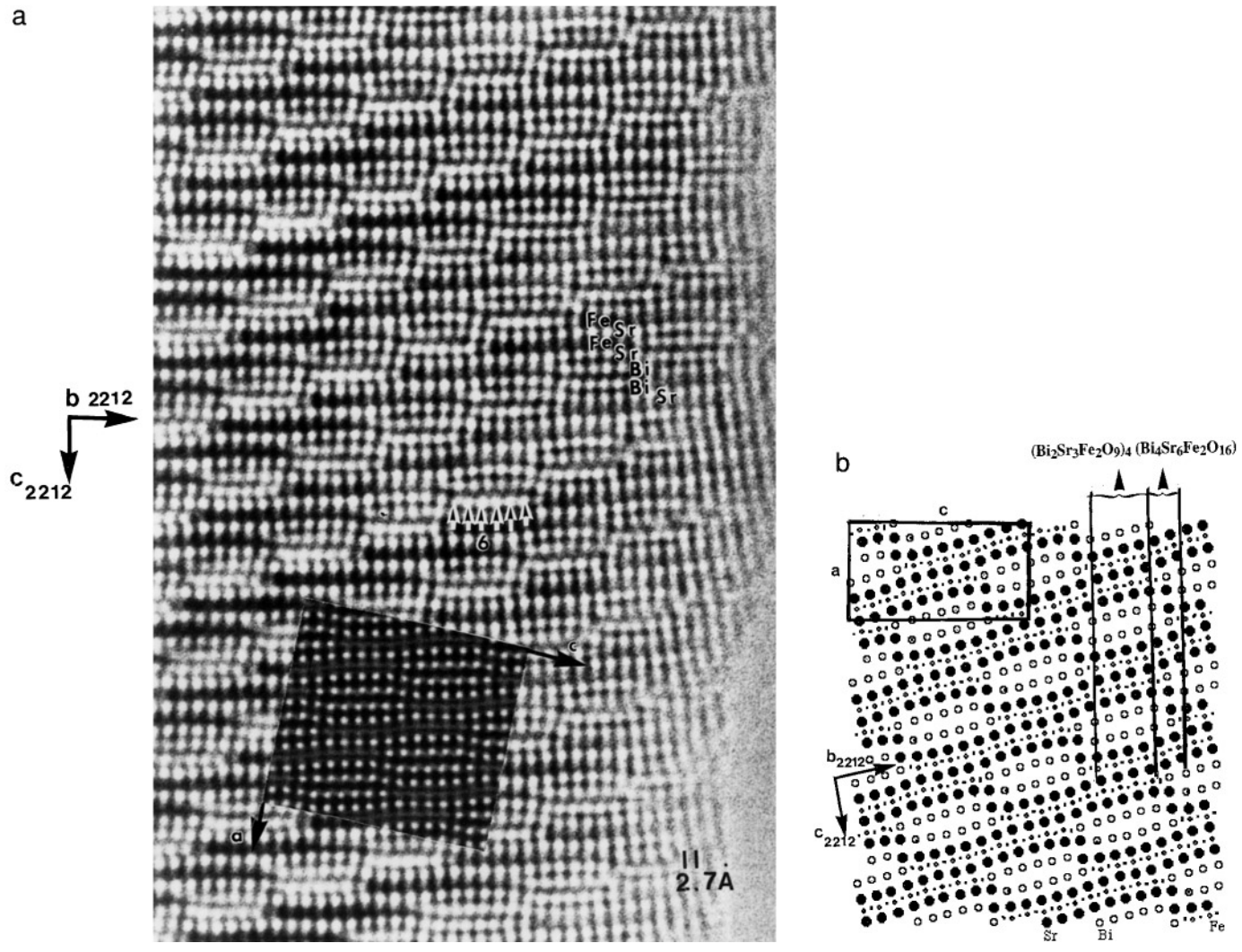

FIG. 2. (a) [010] enlarged HREM image where the heavy electron density zones are highlighted. The nature of the cations is indicated and the six adjacent bismuth atoms are arrowed. The calculated image ($\Delta f = -550$ Å, thickness 25 Å) is in insert. The structure is built up from slices parallel to (001). The $\mathbf{b}_{2212}$ and $\mathbf{c}_{2212}$ axes of the 2212 parent structure are also indicated. (b) Projection of the structure. The monoclinic cell is outlined and the $\mathbf{b}_{2212}$ and $\mathbf{c}_{2212}$ axes indicated. The two types of (001) slices, formulated $[Bi_2Sr_3Fe_2O_9]_4$ and $[Bi_4Sr_6Fe_2O_{16}]$ are shown. The positional parameters are those refined from single crystals (19).

(ii) In the [010] image displayed in Fig. 2a, the rows of very bright spots are correlated to the cation positions in the [SrO] and [BiO] layers whereas the iron layers [FeO_2] appear as rows of small and grey dots. Each slice is six bismuth atoms thick along b_{2212} (see white and black arrows in the middle of the image). Within one (001) ribbon, the stacking sequence of the different ribbons along $\mathbf{c}_{2212}$ is [SrO][BiO][BiO][SrO][FeO_2][SrO][FeO_2]. This sequence is that of the 2212 structure. The structure is therefore generated by shearing mechanisms within a 2212 parent structure.

(iii) The relative orientations of the monoclinic cell and the tetragonal 2212 subcell are:

$$[100]//[0\bar{1}1]_{2212}$$

$$[102]//[010]_{2212}$$

$$[010]//\mathbf{a}_{2212}.$$

The different orientations are indicated in Fig. 2a, b. In the whole paper, the subscripted planes and axes are those of the parent structure; the others refer to the monoclinic cell.

(iv) Referring to the tetragonal 2212 subcell, the shear plane is parallel to $(011)_{2212}$ and the translation roughly $\mathbf{t} = \mathbf{b}_{2212} - 0.13\mathbf{c}_{2212}$ (with b_{2212} and $0.13c_{2212} \approx a_p\sqrt{2}$).

Through this shear plane the rows of metallic atoms face either rows of the same nature or rows of different kind. It results in ribbons that are 6 Bi atoms, 18 Sr atoms, and 10 Fe atoms wide along $\mathbf{b}_{2212}$ (Fig. 2b). Consequently, the cationic sequence along the $\mathbf{b}_{2212}$ direction can be described as "6Bi–18Sr–6Bi–10Fe".

These HREM observations, performed on very regular single crystals, together with the atomic positions refined from single crystal XRD data (19) allow an accurate structure to be established. The structural principle of the latter can be simply described by the stacking along **c** of two kinds of slices, formulated as $[Bi_2Sr_3Fe_2O_9]_4$ and $[Bi_4Sr_6Fe_2O_{16}]$, respectively (Fig. 2b). The first kind of slice, which is four FeO_6 octahedra, i.e., $2a_p\sqrt{2}$, thick along $\mathbf{b}_{2212}$ exhibits the 2212-type structure. The second sort of slice, which ensures the junction between two 2212 slices, is only two FeO_6 octahedra thick; it consists of double perovskite rows, $[SrFeO_3]_\infty$, running along **b**, separated by four double rows containing either strontium or bismuth, with bismuth in trigonal pyramidal coordination. In fact, this particular geometry of the $[Bi_4Sr_6Fe_2O_{16}]_\infty$ slices relates from the mechanism of shearing, which takes place in the 2212 structure along the $(011)_{2212}$ plane.

It is interesting to note that, as a result of the relative arrangement of the six adjacent bismuth atoms, double bismuth segments are formed, as expected for a 2212-type structure. However, these double bismuth segments run over only five octahedra along $\mathbf{b}_{2212}$ because the sequences of six adjacent Bi are shifted by $a_p\sqrt{2}/2$. This is schematically drawn in Fig. 3a, the two extreme Bi atoms facing

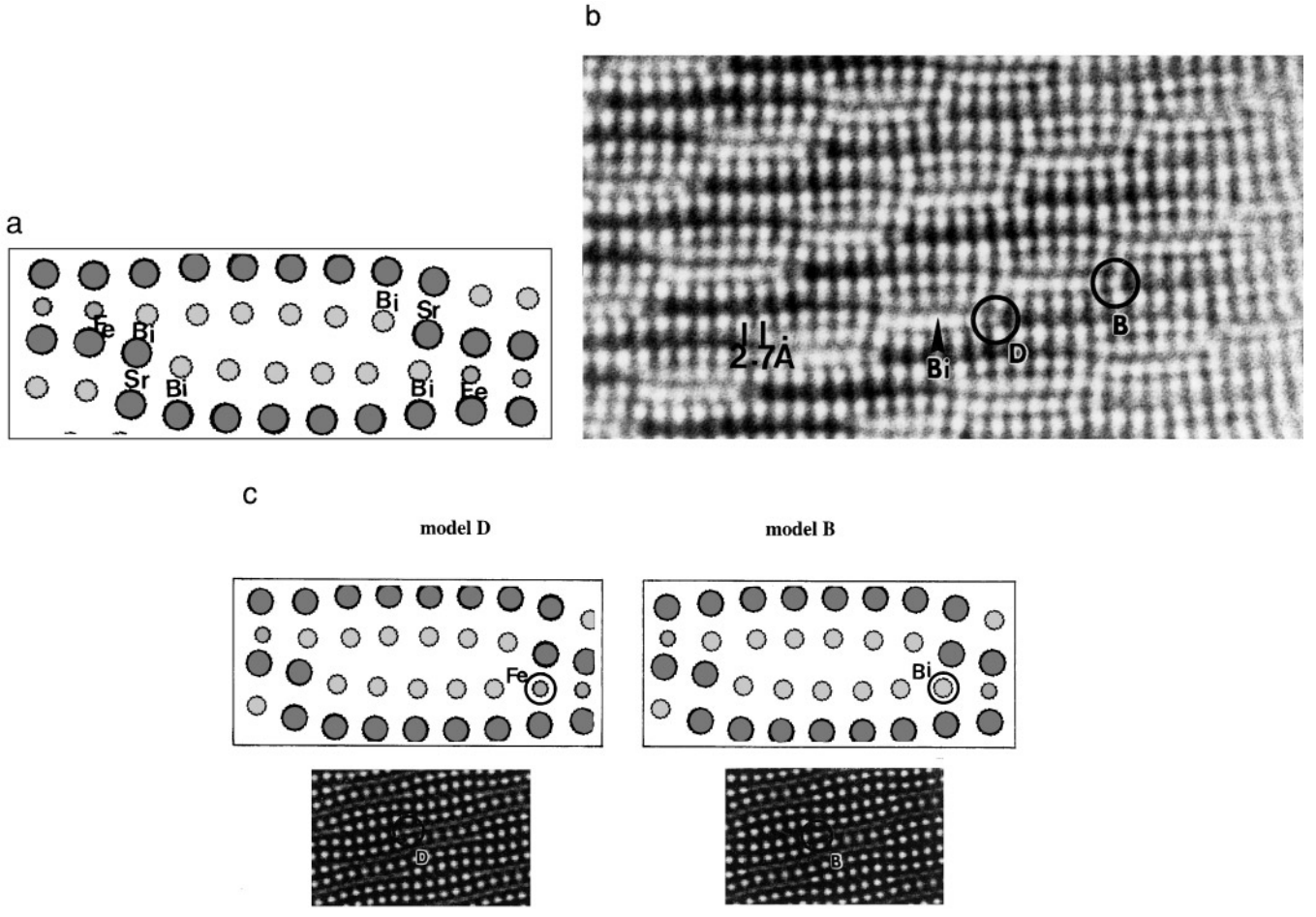

FIG. 3. (a) Drawing of the relative positions of the six bismuth atoms in two adjacent segments which are shifted. The extreme atoms are indicated by black arrowheads (Bi ⇔ Sr) and large black arrows (Bi ⇔ Fe). (b) (010) HREM image, where variations of the contrast is observed at the level of the extreme atoms; two of them are circled. They appear as bright (**B**) or dark (**D**) dots. (c) Calculated images and projections of two limit models corresponding to the Bi/Fe substitution. The model **B** corresponds to the regular structure and the model **D** has the extreme Bi atom is replaced by a Fe atom.

either a Sr or an Fe atom. These double $[Bi_2O_2]_5$ segments are oval shaped, as observed in the 2212 parent structures $Bi_{2+x}Sr_{3-x}Fe_2O_{9+\delta}$, whose modulated structure was recently refined (20), and in other 2201 and 2212 ferrites and cuprates. The displacive modulation of the parent structure results indeed in an undulation of the cationic sheets which is very similar to those described in the 2212 cuprates with an incommensurate component of the modulation vector close to 0.21.

The ideal composition as described above would be $Bi_{24}Sr_{36}Fe_{20}O_{104}$ while the one deduced from EDS analyses corresponds to $Bi_{22}Sr_{35}Fe_{23}O_{104}$, which supposes a small Sr deficiency and iron for Bi substitution.

Nonstoichiometry

The extreme Bi atoms. One of the possible origins of the cation nonstoichiometry is the nature of the atom located at the extremity of the bismuth segments (Fig. 3a). Every segment of six Bi atoms is indeed bordered by a "Sr" segment on one side and by an "Fe" segment on the other side. The extreme atoms are those building the $(011)_{2212}$ double layer located at the level of the shear plane and ensure the connection between the different layers. As previously mentioned, strong variations of contrast are sometimes observed at that level (14, 18). At the junction between a "Bi" and a "Sr" segment (small black arrowheads), the variation of contrast would be scarcely visible because the Sr and Bi atoms exhibit rather close radii and because they adopt a similar environment in the distorted rock salt layer. The situation is different at the junction between a "Bi" and a "Fe" segment (large black arrows) because the distorted BiO_6 (rock salt layer) and FeO_6 (perovskite layer) octahedra are rotated by 45° with respect to each other. Note that the nature of the junction polyhedron has been solved from XRD calculations (19), the extreme Bi exhibiting a fivefold coordination (trigonal bipyramids) in a Fe-type position.

At the level of the extreme Bi/Fe atoms, the spot brightness is highly variable. As an example, a bright spot is circled and labeled **B** in the enlarged image displayed in Fig. 3b, whereas an adjacent spot is darker (circled and labeled **D**). Image calculations were carried out on the basis of a local Fe for Bi substitution (model **D**). The theoretical images calculated for a focus value of -550 Å and a crystal thickness of 22 Å are given in Fig. 3c together with the two corresponding projected models; in both images and models, the substituted atoms are circled. They show that the experimental contrast variation is in perfect agreement with the calculated one and, as a matter of fact, confirm the hypothesis. No ordering of this Bi/Fe substitution feature was detected.

This substitution at the extremity of the bismuth segment is punctual and does not modify the translation of the rest of the structure through the $(001)_{2212}$ shear plane. In that way, one can consider that the actual formulation of the structure is rather $^{\{011\}}[Bi_2Sr_3Fe_2O_9]_4[Bi_{4-x}Sr_6Fe_{2+x}O_{16-\delta}]$.

The $^{\{011\}}[Bi_2Sr_3Fe_2O_9]_m[Bi_{4-x}Sr_6Fe_{2+x}O_{16-\delta}]$ members. Figure 4 represents another type of defect which, in the same way, does not modify the nature of the shearing plane. In a part of a microcrystal, the $(011)_{2212}$ ribbons are well aligned but characterized by variable widths. The double layers separating the 2212 slices are indicated by black triangles in the image. On the crystal edge, the widths of three first 2212-type ribbons become $2.5a_p\sqrt{2}$, $2.5a_p\sqrt{2}$, and $1.5a_p\sqrt{2}$ instead of three times $2a_p\sqrt{2}$. These defects run along **a** throughout the whole matrix. They are simply intergrowth defects and can easily be described as resulting from an increase of the 2212 slice, retaining the $\{011\}_{2212}$ shear planes in the 2212 parent structure. In that way, they correspond to the different members of a structural family which would obey the general formulation $^{\{011\}}[Bi_2Sr_3Fe_2O_9]_m[Bi_{4-x}Sr_6Fe_{2+x}O_{16-\delta}]$. The cells exhibit also a monoclinic symmetry and the a' and b' parameters are similar for each of the members. The regular structure described above would be the member $\mathbf{m} = 4$. In the example displayed in Fig. 4, the defective members observed on the crystal edge are two members with $\mathbf{m} = 5$ and double collapsed 2201/0201 phases, $Bi_{13}Ba_2Sr_{25}Fe_{13}O_{66}$ one with $\mathbf{m} = 3$ (indicated in the image). They exhibit segments of 7 and 5 adjacent bismuth, respectively, instead of six in the regular structure.

Mixed crystallographic shear planes. The existence of defective **m** members within the matrix does not systematically imply the formation of perfect ribbons. As shown in Fig. 5a, viewing at grazing incidence shows that the **m** value of one ribbon sometimes varies along **a**. In this example, the matrix is very regular in the bottom part of the image but, at the level of the defect,one observes that the boundary is shifted locally by $a_p\sqrt{2}/2$. This means that, viewing along **a**, one observes that two adjacent $\mathbf{m} = 4$ members are transformed into one $\mathbf{m} = 5$ and one $\mathbf{m} = 3$ member. In a general way, in such a type of defect, the width of the ribbon is modified with an increment of $\Delta\mathbf{m} = \pm 1$ (i.e., $a_p\sqrt{2}/2$). The existence of these defects implies in fact that the shear plane orientation is locally modified, i.e., is no more $\{011\}_{2212}$.

Defects of this type sometimes extend over a large area. An example of such an area arising in a regular crystal is shown in Fig. 5b (curved white arrow). The progressive variation of the **m** value makes the collapsed boundaries wander in the matrix as a result of the existence of mixed crystallographic shear planes.

Formation of the "3212" member. In spite of the 3D character of the structure, a strong lamellar morphology is

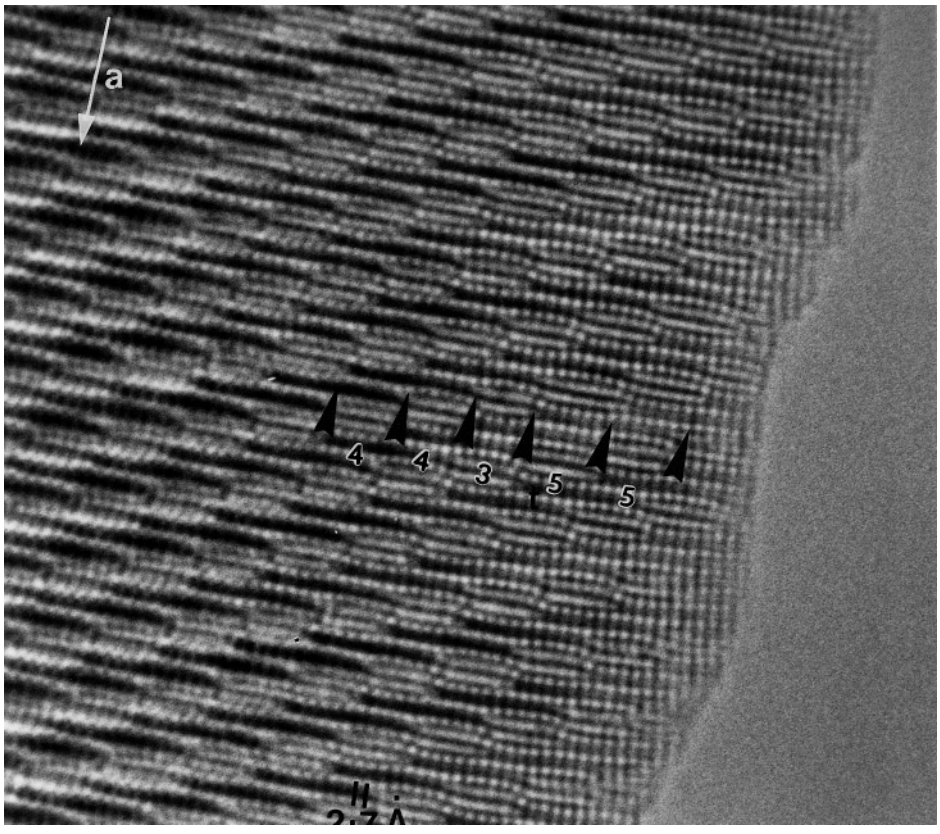

FIG. 4. (010) HREM image where **m** = 5 and **m** = 3 members are observed; they correspond to segments of 7 and 5 bismuth atoms, respectively.

observed. This behavior seems to result from the existence of planar defects parallel to $(001)_{2212}$. An overall image of a highly disturbed crystal is shown in Fig. 6a. One observes intergrowth defects corresponding to variable values of **m**, described in the above sections, but also the existence of large and bright slices running along [101]. They are indicated by large white arrows. The enlarged image of one of these defects is given in Fig. 6b; the zones of high electron density are imaged as bright dots whereas the "Fe" segments appear as dark lines. At the level of the defect, within every ribbon, one observes five segments of bright dots stacked along **a** instead of the four expected for the 2212 parent structure (Sr–Bi–Bi–Sr). The spacing of the corresponding layers corresponds to that of a rock salt-type stacking. This suggests that an additional [*A*O] layer, with *A* = Sr or Bi, is intercalated at the level of the double bismuth layer between the two [SrO] layers, forming locally a layered structure with a quadruple rock salt layer. Such a structure would be a 3212 structure which obeys the ideal formulation $[(Bi, Sr)O]_4\,[SrFeO_3]_2$ (Fig. 6c). Note that the nature of the shear plane is not modified by this type of defect.

These defective slices are not always so perfectly crystallized as those displayed in Fig. 6b. Zones therefore exist where the links are much weaker, which explains the mica-like morphology of the crystallites.

CONCLUDING REMARKS

The HREM study demonstrates the 2212-double collapsed nature of the new ferrite $Bi_{12}Sr_{18}Fe_{10}O_{52}$, whose detailed structure will be described elsewhere (19).

It is remarkable that this ferrite is closely related to the 2212-double collapsed structure of the $Bi_{16}Sr_{28}Cu_{17}O_{69}$ cuprate. In both structures, the nature of the shear plane is the same, $\{011\}$ of the 2212 parent structure, and the ribbons are shifted by the same amplitude. The two structures differ by only the length of the Bi segments and the nature of the perovskite slices, distorted octahedral for the ferrite and pyramidal for the cuprate. The bismuth segments are formed of six adjacent Bi in the ferrite and nine in the cuprate. In this way, $Bi_{12}Sr_{18}Fe_{10}O_{52}$ is the **m** = 4 member of the

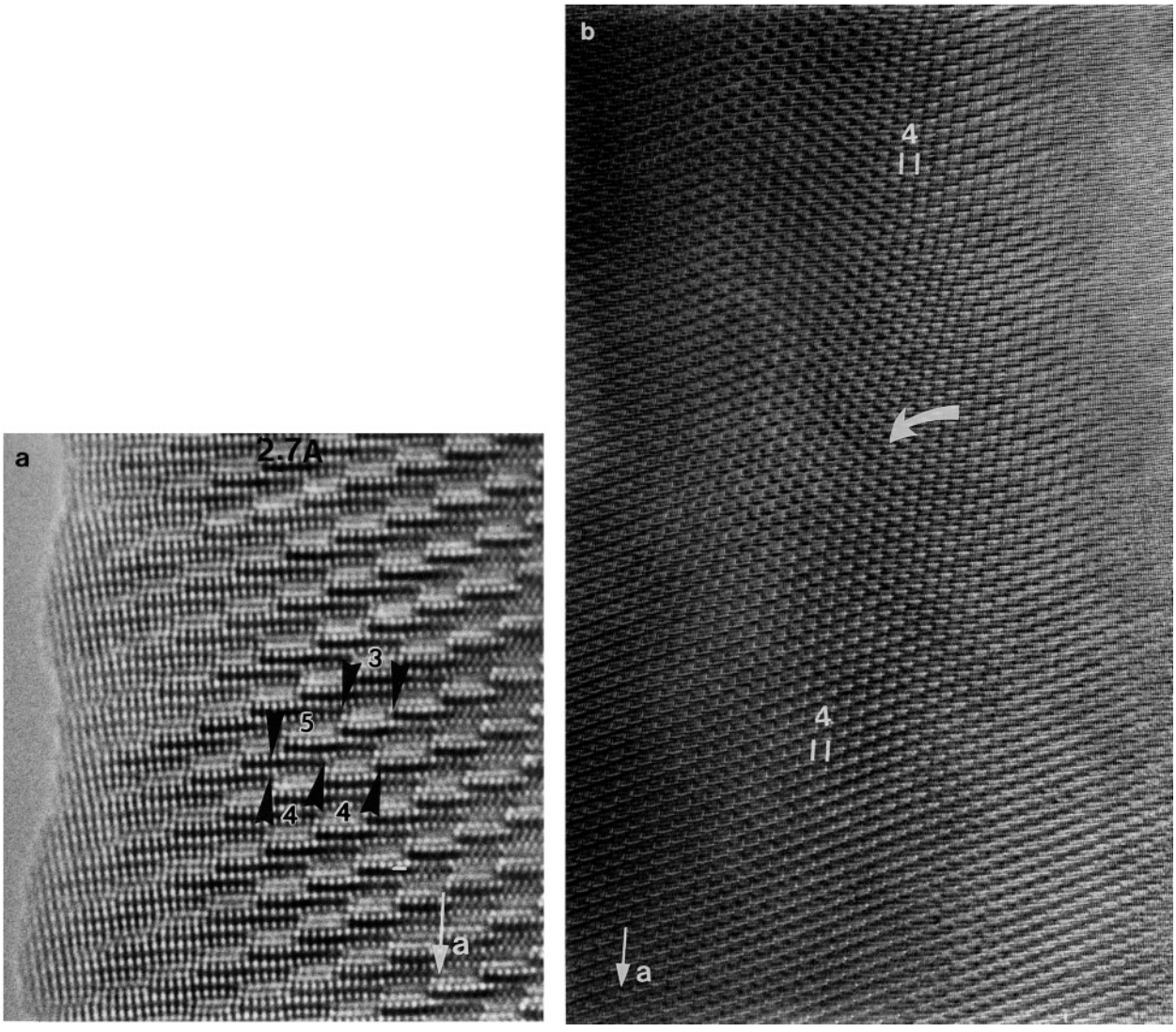

FIG. 5. (a) (010) HREM showing a local variation of the **m** value. On both sides of the local defect, the (011) shear plane is retained. (b) In the middle (curved arrow) of the regular $\mathbf{m} = 4$ crystal, the **m** value changes continuously, leading to wandering boundaries (mixed shear planes).

$^{\{011\}}[Bi_2Sr_3Fe_2O_9]_{\mathbf{m}}[Bi_{4-x}Sr_6Fe_{2+x}O_{16-\delta}]$ family and $Bi_{16}Sr_{28}Cu_{17}O_{69}$ would be the member $\mathbf{m} = 7$ of the homologous family $^{\{011\}}[Bi_2Sr_3Cu_2O_8]_{\mathbf{m}}[Bi_{4-x}Sr_6Cu_{2+x}O_{12+\delta}]$. Considering these ideal formulations, a partial Bi/Sr substitution can also be assumed.

Consideration of the Bi–Sr–Fe–O system (Fig. 7) shows that in this diagram there exist four phases with close compositions and closely related structures: 2212 (1), 2223 (9), the intergrowth 2201–0201 (18), and the 2212-double collapsed (this work). This shows that a small variation of the cationic composition is susceptible to generate new structures by shearing mechanisms, as shown for this new collapsed structure which is clearly bismuth deficient with respect to the 2212 parent structure. Note that similar behavior is observed for the Bi–Sr–Cu–O system, in spite of the different oxygen stoichiometry due to the different valences of copper and iron.

Finally, the observations of imperfect crystallites in the different powder samples, which exhibit ED patterns characteristic of higher **m** members is of great interest. It suggest that different members can be stabilised in the system. Their characterization, which is in progress, should allow to understand the parameters which govern the shearing mechanism and its periodicity.

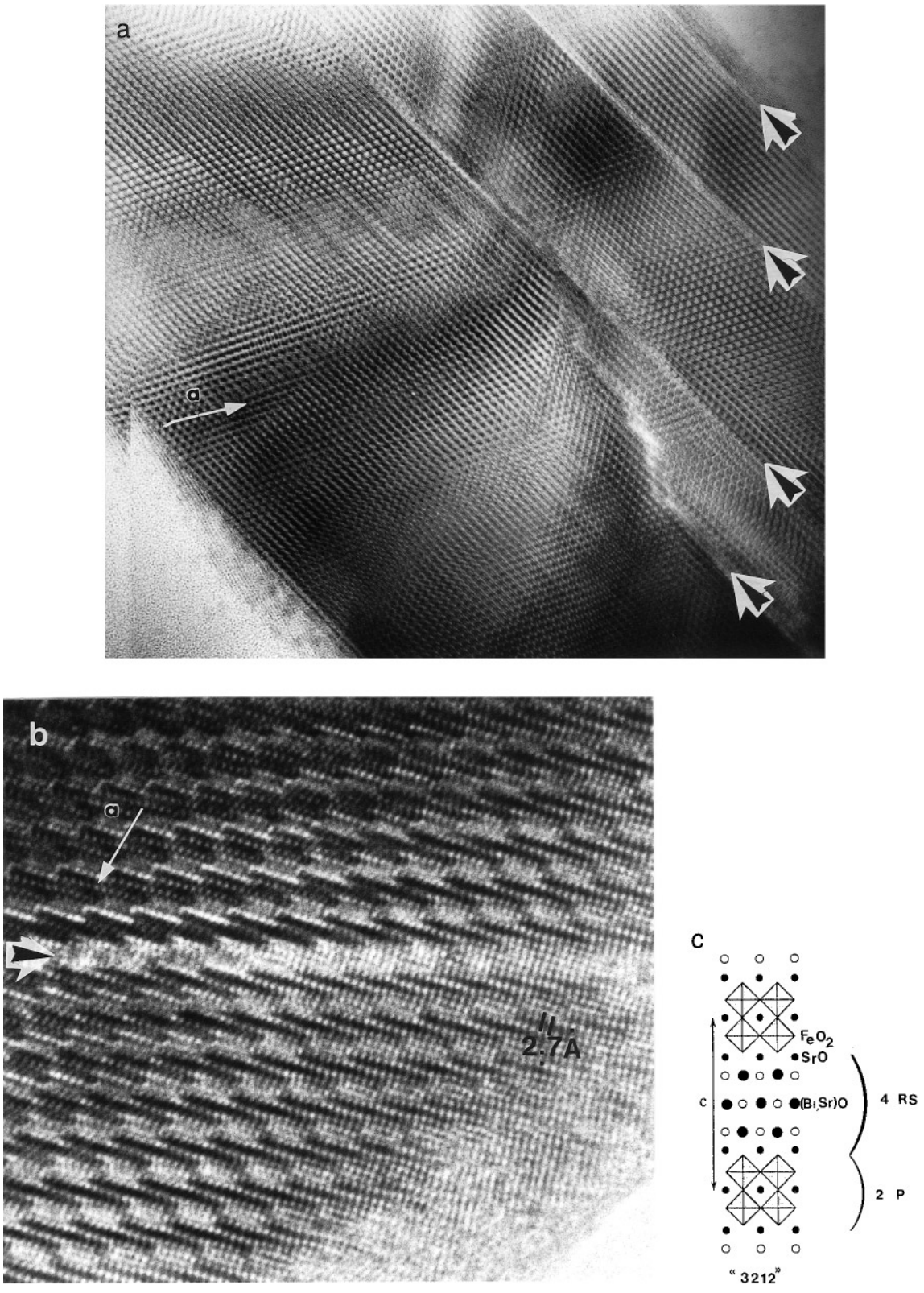

FIG. 6. (a) Overall image of a disturbed crystal. (b) Enlarged image showing the existence of defective slices parallel to (101). They correspond to the intercalation of an additional [(Bi, Sr)O] layer. (c) Idealized drawing of the 3212 structure built up from the intergrowth of a double perovskite layer (2P) and a quadruple rock salt layer (4 RS).

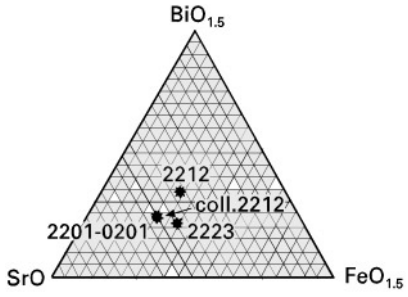

FIG. 7. Ternary diagram, where the layered bismuth strontium ferrites are indicated.

REFERENCES

1. M. Hervieu, C. Michel, N. Nguyen, R. Retoux, and B. Raveau, *Eur. J. Solid State Inorg. Chem.* **25,** 4, 375 (1988).
2. H. Maeda, J. Tanaka, M. Fukutomi, and T. Asano, *Jpn. J. Appl. Phys.* **27,** L209 (1988).
3. J. M. Tarascon, W. R. Mackinnon, P. Barboux, D. M. Hwang, B. G. Bagley, L. H. Greene, G. Hull, Y. Lepage, and N. Stoffel, *Phys. Rev. B* **38,** 8885 (1988).
4. V. Petricek, Y. Gao, P. Lee, and P. Coppens, *Phys. Rev. B* **42,** 42,387 (1990).
5. A. Levin, Y. Smolin, and Y. Shepelev, *J. Phys. Condens. Matter* **6,** 3539 (1994).
6. A. Ruyter, D. Grebille, H. Leligny, P. Labbe, and B. Raveau, *in* "Aperiodic 94," pp. 470. World Scientific, Singapore, 1994.
7. Y. Lepage, W. R. Mc. Kinnon, J. M. Tarascon, and P. Barboux, *Phys. Rev. B* **40,** 6810 (1989).
8. O. Perez, H. Leligny, D. Grebille, P. Labbe, D. Groult, and B. Raveau, *J. Phys. Condens. Matter* **7,** 1003 (1995).
9. R. Retoux, C. Michel, M. Hervieu, N. Nguyen, and B. Raveau, *Solid State Commun.* **69,** 6, 5,599 (1988).
10. M. Takano, Y. Takada, K. Oda, H. Kitaguchi, Y. Miura, Y. Ikeda, Y. Tomii, and H. Mazaki, *Jpn. J. Appl. Phys.* **27,** L1041 (1988).
11. M. Hervieu, D. Pelloquin, C. Michel, M. T. Caldes, and B. Raveau, *J. Solid State Chem.* **118,** 227 (1995).
12. Y. Ikeda, H. Ito, S. Shimomura, Y. Oue, K. Inaba, Z. Hiroi, and M. Takano, *Physica C* **159,** 93 (1989).
13. C. N. R. Rao and B. Raveau, "Transition Metal Oxides." VCH, New York, 1995.
14. M. Hervieu, M. T. Caldes, S. Cabrera, C. Michel, D. Pelloquin, and B. Raveau, *J. Solid State Chem.* **119,** 169 (1995).
15. M. Hervieu, C. Michel, M. T. Caldes, A. Q. Pham, and B. Raveau, *J. Solid State Chem.* **104,** 289 (1993).
16. M. Hervieu, C. Michel, M. T. Caldes, A.Q. Pham, and B. Raveau, *J. Solid State Chem.* **107,** 117 (1993).
17. M. Hervieu, M. T. Caldes, D. Pelloquin, C. Michel, S. Cabrera, and B. Raveau, *J. Mater. Chem.* **6,** 175 (1996).
18. M. Hervieu, C. Michel, M. T. Caldes, C. Michel, D. Pelloquin, and B. Raveau, *J. Solid State Chem.* **118,** 357 (1995).
19. O. Pérez, H. Leligny, D. Grebille, Ph. Labbe, D. Groult, and B. Raveau, *Phys. Rev. B*, in press.
20. O. Pérez, H. Leligny, D. Grebille, J. M. Greneche, Ph. Labbe, D. Groult, and B. Raveau, *Phys. Rev. B*, in press.